Journal of ELECTRONIC MATERIALS, Vol. 50, No. 4, 2021
https://doi.org/10.1007/s11664-020-08629-2


ASIAN CONSORTIUM ACCMS–INTERNATIONAL CONFERENCE ICMG 2020

# Structural and Optical Studies on Strontium-Filled $CoSb_3$ Nanoparticles Via a Solvo-/Hydrothermal Method

M. UDAY KUMAR ,[1,2,3] R. SWETHA,[1,2] and LATHA KUMARI[1,4]

1.—Department of Physics, B.M.S. College of Engineering, Bull Temple Road, Bengaluru, Karnataka 560019, India. 2.—Department of Physics, Mangalore University, Mangalagangothri, Karnataka 574199, India. 3.—e-mail: udaykumar848@gmail.com. 4.—e-mail: lathakumari.phy@bmsce.ac.in

In the present work, strontium-filled $CoSb_3$ nanoparticles ($Sr_yCoSb_3$, y = 0, 0.025, 0.05, 0.075 and 0.1) were synthesized by a solvo-/hydrothermal method. Powder x-ray diffraction (pXRD) analysis reveals a cubic phase of $CoSb_3$ with space group Im $\bar{3}$. The Sr-filled samples show a slight peak shift and broadening of the high-intensity peak at 31.2491° corresponding to the (013) plane which can be attributed to the interaction of Sr atoms filled into voids of the $CoSb_3$ cage-like structure with some of the lattice vibrations in the structure. Field emission scanning electron microscopy (FESEM) images show as-synthesized nanoparticles in the range of 50–160 nm, and energy-dispersive x-ray spectroscopy (EDX) analysis reveals the chemical composition of Sr-filled $CoSb_3$. Fourier transform infrared spectroscopy (FTIR) studies confirm vibrational modes below 1000 $cm^{-1}$ corresponding to Co-Sb and cobalt complexes in both filled and unfilled $CoSb_3$ nanoparticles. UV–Vis absorption analysis indicates a peak shift towards the longer-wavelength region (redshift) and a decrease in the optical band gap as a function of the increase in Sr filling concentration. This can be considered strong evidence for successful filling of voids in the cage-like structure of $CoSb_3$ by strontium.

**Key words:** Skutterudites, nanoparticles, solvo-/hydrothermal, vibrational modes, optical band gap

## INTRODUCTION

In recent years, increased environmental issues such as global warming and worldwide limitations of energy resources have led to efforts towards the development of green energy applications.[1] In this context, thermoelectricity has emerged as a promising technology for the direct and reversible conversion of thermal energy into electrical energy. However, for commercial applications, the use of current thermoelectric (TE) devices is still limited because of their relatively poor efficiency.[2] The efficiency of TE material is determined by the dimensionless figure of merit, $ZT = (S^2\sigma T)/k$, where $S$ is the Seebeck coefficient, $\sigma$ is the electrical conductivity, $T$ is the absolute temperature, and $k$ is the total thermal conductivity ($k = k_{el} + k_{lat}$, where $k_{el}$ and $k_{lat}$ are the electronic and lattice thermal conductivities, respectively). The substantial increase in power factor ($S^2\sigma$) and appreciable reduction in thermal conductivity are expected to enhance the efficiency of thermoelectric devices, which in turn depends mainly on the material properties.[3]

In the past decades, researchers working in the field of thermoelectrics have extensively studied the performance of various thermoelectric materials such as $Bi_2Te_3$, clathrates, skutterudites, $\beta$-$Zn_4Sb_3$, half-Heuslers, Si-Ge and Zintl phases in different temperature regimes.[4–11] Among the various thermoelectric materials studied, skutterudite has been

(Received June 10, 2020; accepted November 17, 2020; published online January 5, 2021)

considered a promising high-efficiency TE material because of its high Seebeck coefficient, high mobility and narrow band gap.[12] Of the various kinds of skutterudites, $CoSb_3$ has garnered much attention because it exhibits good electrical conductivity, a narrow band gap ($\sim$ 0.2 eV) and appreciably high thermal conductivity.[13,14] Recent studies show two effective approaches which have been employed to reduce the lattice thermal conductivity of skutterudite. The first approach is to form a filled skutterudite by inserting guest atoms into voids of the skutterudite structure with various filling atoms such as alkaline earth metals, rare earth metals and others (In, Sn).[15–18] The guest atoms are weakly bonded in the voids, and they act as independent oscillators which effectively scatter heat-carrying phonons in the lattice and significantly reduce the lattice thermal conductivity.[19] Another effective approach is nanostructuring of thermoelectric material, which increases the grain boundaries effectively, thereby scattering the phonons at interfaces and consequently decreasing the phonon thermal conductivity.[20] It has been reported that cerium (rare earth metal) can fill only 10% of the voids in a $CoSb_3$ cage-like structure, whereas indium depicted a filling fraction of 20%. In the present work, strontium (alkaline earth metal) is chosen as filler, which exhibits a filling fraction as high as 40%.[21] Zhao et al.[22] synthesized $Sr_{0.28}Co_4Sb_{12}$ by melting and achieved a maximum $ZT$ of 0.9 at 850 K. Recent studies[23,24] have reported that such compounds have good Seebeck coefficients and that optimization of the chemical composition improves the thermoelectric efficiency. However, the above synthesis method is not cost-effective and requires a long duration, high synthesis temperature and ultra-high vacuum conditions of the order of $10^{-3}$–$10^{-6}$ Torr. For commercial applications, the cost of TE materials production is significant, and short-duration synthesis is also required. In this regard, solvothermal synthesis is considered due to its low synthesis temperature, high reproducibility and low cost.[25,26]

The optical properties of thermoelectrics are seldom reported. $CoSb_3$ has a broad spectral band of linear absorption in the range 300–800 nm which is suitable for nonlinear optical (NLO) applications. Lee et al. reported that filled skutterudites possess good properties for use as topological insulators and they also can be used as broadband saturable absorbers that can cover a bandwidth of 1.5–1.9 $\mu$m.[27] In the present work, a series of $Sr_yCoSb_3$ (y = 0, 0.025, 0.05, 0.075 and 0.1) samples were synthesized by a solvo-/hydrothermal method, and the effects of filling on the structural and optical properties are discussed in detail, with a focus on the optical properties.

## EXPERIMENTAL PROCEDURE

In the present work, a series of $Sr_yCoSb_3$ (y = 0, 0.025, 0.05, 0.075 and 0.1) nanoparticles were synthesized by solvo-/hydrothermal method. Analytically pure $CoCl_2{\cdot}6H_2O$ and $SbCl_3$ were used as starting materials in the molar ratio 1:3 along with $SrCl_2{\cdot}6H_2O$ as filler agent in specified concentrations. A sufficient amount of $NaBH_4$ solution was used as reducing agent. Both solutions were sonicated for 20 min for better dispersion and to obtain homogeneous solution. Reduction reaction was carried out for 15–20 min with manual stirring of the solution. The final solution was transferred into a polypropylene-lined autoclave, which was then filled with *N*,*N*-dimethylformamide (DMF) as a solvent up to 70% of its total volume. The autoclave was carefully sealed and placed in a wide-mouth muffle furnace maintained at 240°C for 24 h. After the reaction period, the autoclave was allowed to cool naturally to room temperature. The obtained precipitate was filtered and washed five to six times with distilled water and ethanol alternatively and repeatedly. Later, as-obtained samples were dried for 10 min at slightly above room temperature to avoid surface oxidation. Further, as-processed materials were filled into a quartz boat and placed in a tubular furnace and annealed at 300°C for 5 h in the presence of an inert (argon) atmosphere.

The phase purity of the as-prepared TE materials was examined by powder x-ray diffraction (pXRD) using a Rigaku Ultima IV powder x-ray diffractometer equipped with Cu $K_\alpha$ radiation ($\lambda$ = 1.5406 Å). The data was recorded with a scan rate of 2 degrees/min. The surface morphology and chemical composition of the TE materials were observed by using a JEOL JSM-7100F field emission scanning electron microscope (FESEM) embedded with an energy-dispersive x-ray (EDX) spectrometer. Fourier transform infrared (FTIR) spectra were recorded at room temperature in the range 400–4000 $cm^{-1}$ in KBr medium using a Perkin Elmer spectrometer. Absorption spectra were recorded in the wavelength range of 200–800 nm with a Perkin Elmer UV/VIS LAMBDA 365 instrument.

## RESULTS AND DISCUSSION

### A. Surface morphology of unfilled and Sr-filled $CoSb_3$ nanoparticles

Figure 1a shows the FESEM image of $CoSb_3$ nanoparticles synthesized by solvo-/hydrothermal method at 240°C for 24 h. Surface morphology images depict block-like nanoparticles with average grain diameters of about 80–230 nm. Figure 1b

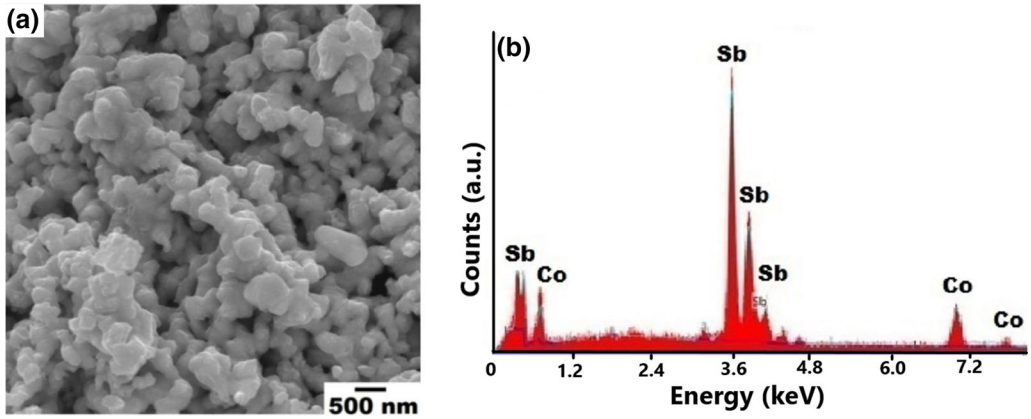


Fig. 1. (a) FESEM image of $CoSb_3$ nanoparticles and (b) EDX spectrum.

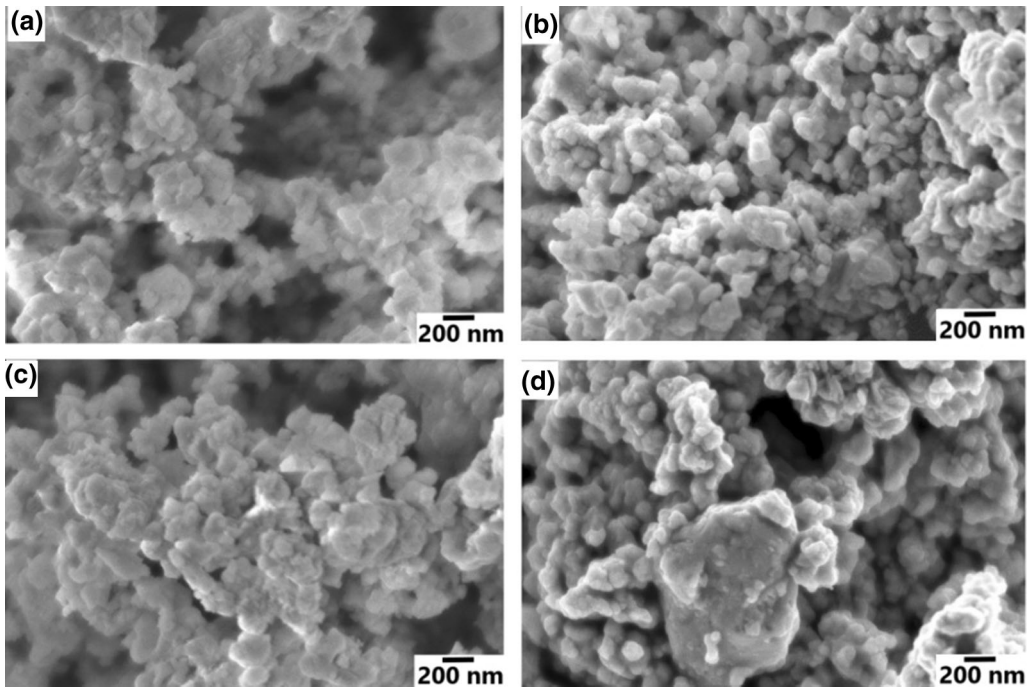


Fig. 2. (a–d) FESEM images of $Sr_yCoSb_3$ (y = 0.025, 0.05, 0.075 and 0.1) nanoparticles.

represents the EDX spectrum of $CoSb_3$ nanoparticles, depicting the chemical composition of the as-synthesized nanoparticles with stoichiometric composition of Co and Sb and no impurity peaks, which confirms the purity of the sample. Our previous work[26] discussed the effect of additive/surfactant on the surface morphology of $CoSb_3$ samples, where nanoparticles as small as 10 nm with narrow particle size distribution were obtained.

Figure 2a, b, c, and d represent the FESEM images of strontium-filled $CoSb_3$ nanoparticles with specified filling concentration. As compared to the unfilled $CoSb_3$, the filled $CoSb_3$ shows dramatic reduction in the particle size and average grain diameter of about 50–120 nm. Similar particle size reduction was observed in indium-[28] and cerium-filled[29] $CoSb_3$ samples. The reduced grain size is

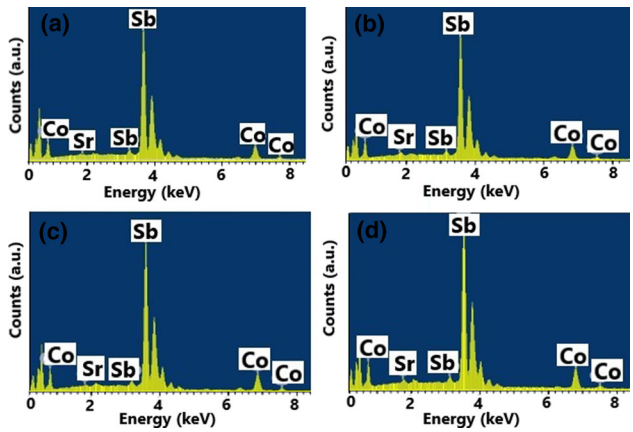


Fig. 3. (a–d) EDX spectra of $Sr_yCoSb_3$ (y = 0.025, 0.05, 0.075 and 0.1) nanoparticles.

expected to consequently increase the grain boundaries and thereby reduce the phonon thermal conductivity of the material.[20] Figure 3 presents the EDX spectrum of Sr-filled $CoSb_3$ nanoparticles, which confirms the presence of Co, Sb and Sr elements. This result justifies the possible effect of strontium filling into the voids of the $CoSb_3$ structure.

B. Structural characterization of unfilled and Sr-filled $CoSb_3$ nanoparticles

Figure 4a displays the x-ray intensity patterns of $Sr_yCoSb_3$ (y = 0, 0.025, 0.05, 0.075 and 0.1). A majority of the diffraction peaks match with standard data (JCPDS: 76-0470) assigned for the cubic phase of $CoSb_3$ with space group Im $\bar{3}$. However, the diffraction data also depict few peaks of secondary phases which can be attributed to CoSb, $CoSb_2$ and Sb. Our previous work[26] on the additive-based synthesis of $CoSb_3$ nanoparticles also reports the presence of traces of secondary phases. Mi et al.[30] reported that the formation of $CoSb_3$ takes place in a stepwise manner, and secondary phases (CoSb, $CoSb_2$ and Sb) act as intermediate products before the formation of $CoSb_3$ phase. The possible chemical reactions during the formation of $CoSb_3$ can be written as:

$$CoCl_2 + 2NaBH_4 \rightarrow Co + 2BH_3 + 2NaCl + H_2 \quad (1)$$

$$2SbCl_3 + 6NaBH_4 \rightarrow 2Sb + 6BH_3 + 6NaCl + 3H_2 \quad (2)$$

$$Co + Sb \rightarrow CoSb \quad (3)$$

$$CoSb + Sb \rightarrow CoSb_2 \quad (4)$$

$$CoSb_2 + Sb \rightarrow CoSb_3 \quad (5)$$

During the reduction reaction, the strong reducing agent $NaBH_4$ rapidly and completely reduces $Co^{2+}$ and $Sb^{3+}$ into Co and Sb as represented in Eqs. 1 and 2. Therefore, formed CoSb will react with Sb atoms to form $CoSb_2$ and then with active Sb atoms to form $CoSb_3$ phase. For all filled samples, broadening of a high-intensity peak at 31.2491° corresponding to the (013) plane and variation in peak intensity for the (220) plane is observed, which may be due to the random distribution of strontium atoms at the void positions.[31,32] Also, all diffraction peaks gradually shift towards higher angles, as shown in Fig. 4b. This result indicates that strontium is successfully filled into the voids of $CoSb_3$ without distracting its original cubic crystal structure. The diffraction peaks corresponding to the $CoSb_2$ impurity phase still persisted in indium-filled samples,[28] whereas they almost disappeared with an increase in the cerium[29] filling concentration, as observed in our previous works. Using Bragg's law, lattice constants of the unfilled and Sr-filled samples were calculated and tabulated in Table I. From Table I, it is observed that the lattice constant of the unfilled $CoSb_3$ is 9.0504 Å which agrees well with the reported value (9.0551Å) for cubic $CoSb_3$ skutterudite.[33] Also, with an increasing filling concentration, the lattice constant linearly decreases due to the small lattice constant of the strontium and peak shift towards higher angles.[28] It is also observed that except for small peak shifts and the occurrence of less intense secondary phases, no substantial variation in the XRD patterns of filled samples is observed. However, these secondary phases are often expected to transform to $CoSb_3$ phase when subjected to sample processing techniques such as hot pressing (HP) or spark plasma sintering (SPS) before the samples are considered for transport property measurements.[15]

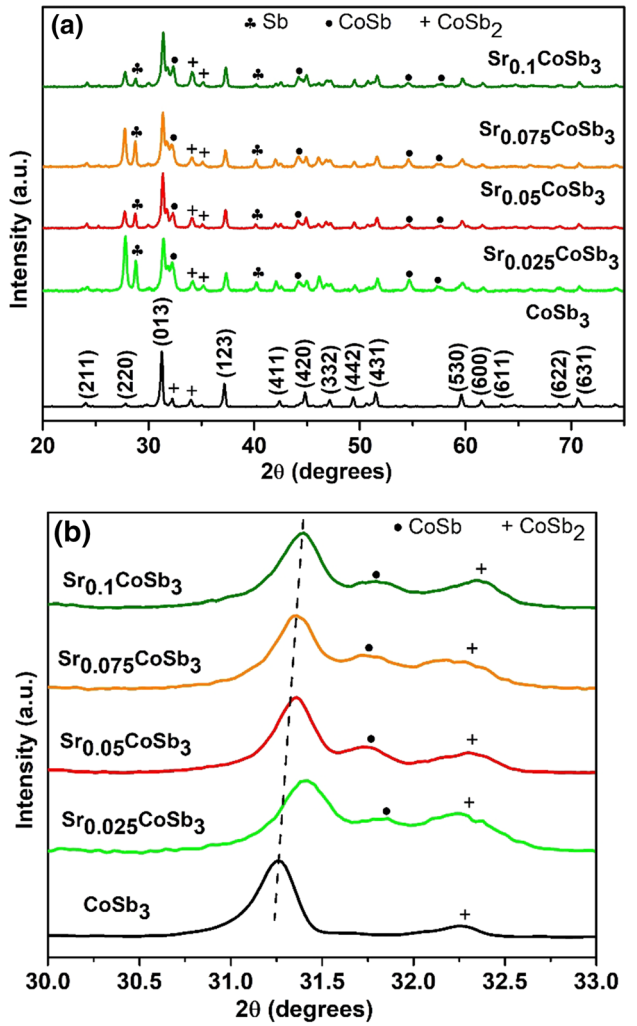


Fig. 4. (a) X-ray intensity patterns of $Sr_yCoSb_3$ (y = 0, 0.025, 0.05, 0.075 and 0.1) nanoparticles. (b) Peak shift at higher diffraction angles as a function of variation in strontium concentration.

**Table I. The *d*-spacing, lattice parameter and crystallite size of $Sr_yCoSb_3$ (y = 0, 0.025, 0.05, 0.075 and 0.1) samples**

| Nominal composition | 2θ (°) | *d*-spacing (Å) | Lattice parameter a (Å) | Crystallite size $D_p$ (nm) |
|---|---|---|---|---|
| $CoSb_3$ | 31.2491 | 2.8620 | 9.0504 | 41.75 |
| $Sr_{0.025}CoSb_3$ | 31.3757 | 2.8488 | 9.0086 | 28.00 |
| $Sr_{0.05}CoSb_3$ | 31.3504 | 2.8509 | 9.0153 | 39.12 |
| $Sr_{0.075}CoSb_3$ | 31.3424 | 2.8517 | 9.0178 | 35.62 |
| $Sr_{0.1}CoSb_3$ | 31.3850 | 2.8479 | 9.0058 | 34.21 |

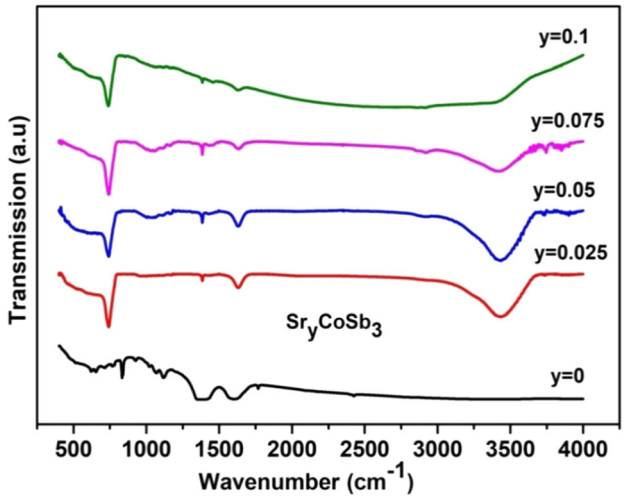


Fig. 5. FTIR spectra of $Sr_yCoSb_3$ (y = 0, 0.025, 0.05, 0.075 and 0.1) nanoparticles.

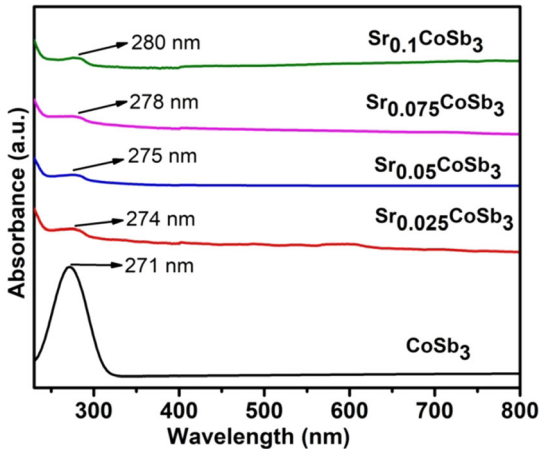


Fig. 6. UV–visible spectra of $Sr_yCoSb_3$ (y = 0, 0.025, 0.05, 0.075 and 0.1) nanoparticles.

### C. FTIR spectrum analysis of unfilled and Sr-filled $CoSb_3$ nanoparticles

Figure 5 shows the FTIR transmittance spectra of $Sr_yCoSb_3$ (y = 0, 0.025, 0.05, 0.075 and 0.1) nanoparticles in the range 400–4000 $cm^{-1}$. The whole spectrum is divided into four regions and is analyzed as follows. Especially in the first region, the peaks in the range 621–925 $cm^{-1}$ can be ascribed to cobalt complex and Co-Sb bonding. For all the filled samples, a single prominent peak is found around 740 $cm^{-1}$ which can be anticipated to arise due to Sr filling into voids of $CoSb_3$ and also may be due to nanoparticles.[34] In the second region, the peaks around 1112–1384 $cm^{-1}$ can be assigned to cobalt complex and O–H in-plane bending. In the third region, peaks around 1600–1767 $cm^{-1}$ can be ascribed to metal–oxygen bonding, and in the fourth region, the broad absorption peak about 3431 $cm^{-1}$ is assigned to the O–H functional group.[35] From Fig. 5, it is also observed that with increasing filling concentration, there is slight variation in position and intensity, but no substantial effect on the vibrational modes in $CoSb_3$ structure.[32]

### D. Optical characterization of unfilled and Sr-filled $CoSb_3$ nanoparticles

Figure 6 shows a typical UV–visible absorption spectra of $Sr_yCoSb_3$ (y = 0, 0.025, 0.05, 0.075 and 0.1) nanoparticles in the wavelength range 200–800 nm. From the absorption spectra, it is observed that all the samples show a single absorption peak in the wavelength range of 271–280 nm, and there is no absorption peak found in the range of 300–700 nm, indicating that such materials are suitable for nonlinear optical (NLO) applications.[29,36] The additive-based $CoSb_3$ nanoparticles and indium- and cerium-filled $CoSb_3$ depict similar UV–visible absorption spectra.[26,28,29] From Fig. 6, it is also noticed that for all the filled samples, the absorption peak shifts towards the longer-wavelength region (redshift), and the peak intensity also decreases, which may be due to nanostructuring. This analysis can be considered as confirmation of the successful filling of strontium into the voids of $CoSb_3$ structure.[37] Using the absorption edge, the direct and indirect optical band gap were calculated as shown in Fig. 7.

The optical band gap is determined by a Tauc plot using the following equation

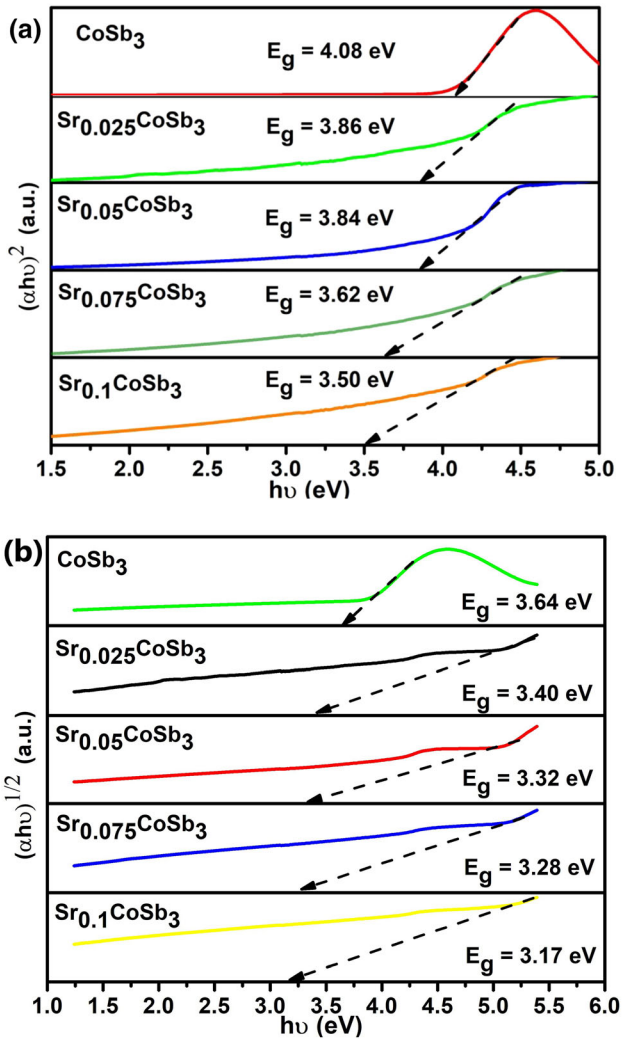


Fig. 7. (a) Plot of $(\alpha h\nu)^2$ versus $h\nu$ for direct band gap. (b) Plot of $(\alpha h\nu)^{1/2}$ versus $h\nu$ for indirect band gap.

$$(\alpha h\nu) = \mathrm{B}(h\nu - E_g)^n \quad (6)$$

where $\alpha$ is the absorption coefficient, B is a constant, $h\nu$ is the energy of incident photons, $E_g$ is the optical band gap energy, and $n$ = 1/2 and 2 for direct and indirect allowed transitions, respectively. Plots of $(\alpha h\nu)^2$ versus $h\nu$ and $(\alpha h\nu)^{1/2}$ versus $h\nu$ at $(\alpha h\nu)^2 = 0$ and $(\alpha h\nu)^{1/2} = 0$ give the direct and indirect band gaps, respectively, which are shown in Fig. 7a and b. For $Sr_yCoSb_3$ (y = 0, 0.025, 0.05, 0.075 and 0.1) nanoparticles, direct allowed transition ($n$ = 1/2) lies between 3.50 eV and 4.08 eV, while indirect allowed transition ($n$ = 2) lies between 3.17 eV and 3.64 eV.

The variations in direct and indirect optical band gap as a function of Sr filling fraction are as shown in Fig. 8. It can be seen that both direct and indirect band gap decrease with an increase in filling concentration because of phonon interaction and also shifting of absorption peak towards the longer-wavelength region.[38]

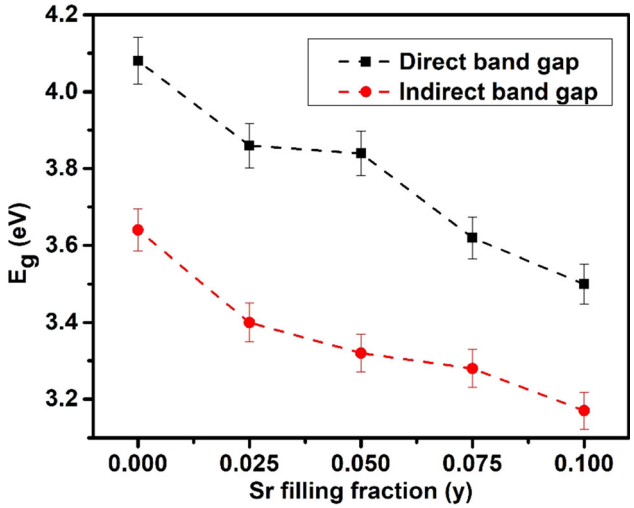


Fig. 8. Variation of direct and indirect band gap for $Sr_yCoSb_3$ (y = 0, 0.025, 0.05, 0.075 and 0.1).

## CONCLUSION

In summary, Sr-filled and unfilled $CoSb_3$ nanoparticles were successfully synthesized by a solvo-/hydrothermal method. pXRD analysis confirms the cubic structure of $CoSb_3$, and it also shows the broadening of some prominent peaks, which can be attributed to the effect of Sr filling of the $CoSb_3$ void structure. Surface morphology images show block-like nanoparticles with an average size of 80–230 nm for un-filled $CoSb_3$ and 50–120 nm for Sr-filled $CoSb_3$ samples. FTIR spectra for un-filled and filled $CoSb_3$ present vibrational modes below 1000 $cm^{-1}$ which can be assigned to Co-Sb and cobalt complexes. The UV–Vis absorption spectrum shows absorption peak shift towards the longer-wavelength region (redshift). The decreases in the optical band gap can be attributed to the interaction of Sr atoms filled into the voids of the $CoSb_3$ crystal structure with the lattice phonons in the skutterudite and also due to nanostructuring.

## ACKNOWLEDGMENTS

This work was supported by VGST GoK K-FIST (Level 1) under Grant No. VGST/GRD-552-/2016-17/2017-18. The authors would like to thank the Department of Chemistry and Department of Physics, B.M.S. College of Engineering for UV–visible absorption spectroscopy and FTIR measurement facilities, respectively. We extend our thanks to the Centre for Nano and Material Sciences, Jain University for the pXRD characterization facility under the NANOMISSION PROJECT "SR/NM/NS-20/2014" and DST-PURSE Laboratory, Mangalore University for providing the FESEM-EDX facility.

## CONFLICT OF INTEREST

The authors declare that they have no known competing financial interests or personal relation-

ships that could have appeared to influence the work reported in this paper.

## REFERENCES


1. X.F. Zheng, C.X. Liu, Y.Y. Yan, and Q. Wang, *Renew Sust. Energ Rev.* 32, 486 (2014).
2. L.E. Bell, *Science* 321, 1457 (2008).
3. G.H. Kim, L. Shao, K. Zhang, and K.P. Pipe, *Nat. Mater.* 12, 719 (2013).
4. S.I. Kim, K.H. Lee, H.A. Mun, H.S. Kim, S.W. Hwang, J.W. Roh, D.J. Yang, W.H. Shin, X.S. Li, Y.H. Lee, G.J. Snyder, and S.W. Kim, *Science* 348, 109 (2015).
5. S. Wang, H. Li, R. Lu, G. Zheng, and X. Tang, *Nanotechnology* 24, 285702 (2013).
6. A. Saramat, G. Svensson, A.E.C. Palmqvist, C. Stiewe, E. Mueller, D. Platzek, S.G.K. Williams, D.M. Rowe, J.D. Bryan, and G.D. Stucky, *J. Appl. Phys.* 99, 023708 (2006).
7. T. Caillat, J.P. Fleurial, and A. Borshchevsky, *J. Phys. Chem. Solids* 58, 1119 (1997).
8. G. Rogl and P. Rogl, *Curr. Opin. Green Sustain. Chem.* 4, 50 (2017).
9. X. Yan, W. Liu, H. Wang, S. Chen, J. Shiomi, K. Esfarjani, H. Wang, D. Wang, G. Chen, and Z. Ren, *Energy Environ. Sci.* 5, 7543 (2012).
10. X.W. Wang, H. Lee, Y.C. Lan, G.H. Zhu, G. Joshi, D.Z. Wang, J. Yang, A.J. Muto, M.Y. Tang, J. Klatsky, S. Song, M.S. Dresselhaus, G. Chen, and Z.F. Ren, *Appl. Phys. Lett.* 93, 193121 (2008).
11. E.S. Toberer, C.A. Cox, S.R. Brown, T. Ikeda, A.F. May, S.M. Kauzlarich, and G.J. Snyder, *Adv. Funct. Mater.* 18, 2795 (2008).
12. J.O. Sofo and G.D. Mahan, *Phys. Rev. B* 58, 15620 (1998).
13. C. Uher, *Semicond. Semimet.* 69, 139 (2001).
14. B.C. Sales, D. Mandrus, B.C. Chakoumakos, V. Keppens, and J.R. Thompson, *Phys. Rev. B* 56, 15081 (1997).
15. Y.Z. Pei, J. Yang, L.D. Chen, W. Zhang, J.R. Salvador, and J. Yang, *Appl. Phys. Lett.* 95, 042101 (2009).
16. L.D. Chen, T. Kawahara, X.F. Tang, T. Goto, T. Hirai, J.S. Dyck, W. Chen, and C. Uher, *J. Appl. Phys.* 90, 1864 (2001).
17. G.S. Nolas, M. Kaeser, R.T. Littleton IV, and T.M. Tritt, *Appl. Phys. Lett.* 77, 1855 (2000).
18. H. Liu, H. Gao, Y. Gu, and X. Zhao, *J. Rare Earths* 29, 596 (2011).
19. E.S. Toberer, A. Zevalkink, and G.J. Snyder, *J. Mater. Chem.* 21, 15843 (2011).
20. Z.G. Chen, G. Han, L. Yang, L. Cheng, and J. Zou, *C-MRS* 22, 535 (2012).
21. X. Shi, S. Bai, L. Xi, J. Yang, W. Zhang, and L. Chen, *J. Mater. Res.* 26, 1745 (2011).
22. X.Y. Zhao, X. Shi, L.D. Chen, W.Q. Zhang, W.B. Zhang, and Y.Z. Pei, *J. Appl. Phys.* 99, 053711 (2006).
23. S.Q. Bai, X.Y. Zhao, Y.Z. Pei, L.D. Chen, and W.Q. Zhang, *IEEE 25th International Conference on Thermoelectrics*, 145 (2006).
24. X. Zhao, X. Shi, L. Chen, S.Q. Bai, W.B. Zhang, and X. Tang, *Eng. Mater.* 336, 842 (2007).
25. A. Gharleghi, Y.H. Pai, F.H. Lin, and C.J. Liu, *J. Mater. Chem.* 2, 4213 (2014).
26. L. Kumari, W. Li, J. Huang, and P.P. Provencio, *Nanoscale Res. Lett.* 5, 1698 (2010).
27. J. Lee, B.K. Yu, Y.I. Jhon, J. Koo, S.J. Kim, Y.M. Jhon, and J.H. Lee, *Adv. Optical Mater.* 5, 1700096 (2017).
28. M.U. Kumar, R. Swetha, and L. Kumari, *J. Phys Conf. Ser.* 1495, 012006 (2020).
29. R. Swetha, M.U. Kumar, and L. Kumari, *AIP Conf. Proc.* 2162, 020104 (2019).
30. J.L. Mi, X.B. Zhao, T.J. Zhu, J.P. Tu, and G.S. Cao, *J. Alloys Compd.* 417, 269 (2006).
31. X. Shi, W. Zhang, L.D. Chen, and C. Uher, *Int. J. Mat. Res.* 99, 638 (2008).
32. M.U. Kumar, R. Swetha, M.V. Murugendrappa, and L. Kumari, *AIP Conf. Proc.* 2162, 020054 (2019).
33. T.H. Schmidt, G. Kliche, and H.D. Lutz, *Acta. Cryst. C* 43, 1678 (1987).
34. S.B. Mary and A.L. Rajesh, *IJSRST* 3, 140 (2017).
35. S. Ariponnammal and R. Velvizhi, *Res. J. Recent Sci.* 3, 332 (2014).
36. A. Jamal, M.M. Rahman, S.B. Khan, M. Faisal, K. Akhtar, M.A. Rubb, A.M. Asiri, and A.O. Al-Youbi, *Appl. Surf. Sci.* 261, 52 (2012).
37. D. Mohanta, N. Mishra, and A. Choudhury, *Mater. Lett.* 58, 3694 (2004).
38. V. Sharma, S.P. Singh, G.S. Mudahar, and K.S. Thind, *New J. Glass Ceram.* 2, 133 (2012).